

Structural Reliability Assessment by a Modified Spectral Stochastic Meshless Local Petrov-Galerkin Method

Guang Yih Sheu^{1,2}

¹Department of Accounting and Information System, Chang-Jung Christian University, Tainan, Chinese Taipei

²Department of Civil Engineering, Feng-Chia University, Taichung, Chinese Taipei

Email: xsheu@hotmail.com

Received January 29, 2013; revised March 9, 2013; accepted March 16, 2013

Copyright © 2013 Guang Yih Sheu. This is an open access article distributed under the Creative Commons Attribution License, which permits unrestricted use, distribution, and reproduction in any medium, provided the original work is properly cited.

ABSTRACT

This study presents a new tool for solving stochastic boundary-value problems. This tool is created by modify the previous spectral stochastic meshless local Petrov-Galerkin method using the MLPG5 scheme. This modified spectral stochastic meshless local Petrov-Galerkin method is selectively applied to predict the structural failure probability with the uncertainty in the spatial variability of mechanical properties. Except for the MLPG5 scheme, deriving the proposed spectral stochastic meshless local Petrov-Galerkin formulation adopts generalized polynomial chaos expansions of random mechanical properties. Predicting the structural failure probability is based on the first-order reliability method. Further comparing the spectral stochastic finite element-based and meshless local Petrov-Galerkin-based predicted structural failure probabilities indicates that the proposed spectral stochastic meshless local Petrov-Galerkin method predicts the more accurate structural failure probability than the spectral stochastic finite element method does. In addition, generating spectral stochastic meshless local Petrov-Galerkin results are considerably time-saving than generating Monte-Carlo simulation results does. In conclusion, the spectral stochastic meshless local Petrov-Galerkin method serves as a time-saving tool for solving stochastic boundary-value problems sufficiently accurately.

Keywords: Spectral Stochastic Meshless Local Petrov-Galerkin Method; Generalized Polynomial Chaos Expansion; First-Order Reliability Method; Structural Failure Probability; Reliability Index

1. Introduction

Available stochastic numerical methods for solving stochastic boundary-value problems include the Monte Carlo simulation, spectral stochastic finite element [1] and stochastic element-free Galerkin methods [2]. The Monte Carlo simulation may be simplest, since implementing it requires sampling the existing random fields and substituting the resulting samples into deterministic solutions. However, a requisite of obtaining accurate Monte Carlo simulation results is sufficiently sampling the existing random fields; therefore, completing a Monte Carlo simulation is usually time-consuming. This requisite brings about a motive of developing a time-saving tool for solving stochastic boundary-value problems.

Meanwhile, the spectral stochastic finite element or stochastic element-free Galerkin methods are developed by extending the finite element or element-free Galerkin methods. For example, deducing a spectral stochastic finite element couples a finite element formulation with such as polynomial chaos and Karhunen-Loève expansions of

stochastic processes. These stochastic processes are assumed to represent the existing uncertainty.

A number of spectral stochastic finite element formulations are available for some branches in engineering science and mechanics. References [3,4] are two recent examples. Nevertheless, applying these two stochastic numerical methods needs a finite element discretization or background cells for the numerical integration. To provide more freedom in solving stochastic boundary-value problems, a truly-meshless stochastic numerical method may be a promising alternative. In a published study [5], a spectral stochastic meshless local Petrov-Galerkin method has been developed by coupling a meshless local Petrov-Galerkin formulation and radial basis function-based meshfree shape functions with polynomial chaos expansions [6] of stochastic processes. Since the meshless local Petrov-Galerkin method is truly meshless [7], the spectral stochastic meshless local Petrov-Galerkin method is also truly meshless. Nonetheless, the spectral stochastic meshless local Petrov-Galerkin results of two elastostatic problems are more accurate than spectral

stochastic finite element results of the same problems. In addition, generating the spectral stochastic meshless local Petrov-Galerkin results is considerably time-saving.

Based on the published conclusion [8] that the MLPG5 scheme may substitute for the finite element method to solve boundary-value problems, the current study further derives a two-dimensional spectral stochastic meshless local Petrov-Galerkin formulation in elastostatics using the MLPG5 scheme. The resulting spectral stochastic meshless local Petrov-Galerkin formulation is selectively applied to predict the structural failure probability with the uncertainty in the spatial variability of mechanical properties. In addition to the MLPG5 scheme, deriving the proposed spectral stochastic meshless local Petrov-Galerkin formulation adopts the generalized polynomial chaos expansions [6] of random mechanical properties and radial basis function-based meshless shape functions. Meanwhile, predicting the structural failure probability is based on the first-order reliability method [9].

The remainder of this study is organized in 5 sections. In Section 2, deriving a meshless local Petrov-Galerkin formulation in elastostatics using the MLPG5 scheme is presented. In Section 3, coupling the resulting expressions in Section 2 with generalized polynomial chaos expansions of random mechanical properties to deduce a spectral stochastic meshless local Petrov-Galerkin formulation is presented. In Section 4, the algorithm for implementing the first-order reliability method is reviewed. Section 5 inspects the accuracy of spectral stochastic meshless local Petrov-Galerkin-based results. Based on this inspection, Section 6 presents the conclusion.

2. Meshless Local Petrov-Galerkin Formulation

Suppose the linearly elastic and isotropic material. In addition, the infinitesimal strain assumption holds. Describe any physical parameter as functions of \mathbf{x} and $\boldsymbol{\theta}$ within a problem domain Ω in which $\mathbf{x} = (x_1, x_2)$ is a vector of spatial coordinates and $\boldsymbol{\theta}$ is an event in the probability space. The succeeding study introduces the stress equations of equilibrium to derive a meshless local Petrov-Galerkin formulation. These stress equations have the following tensor form [10]:

$$\sigma_{ij,j} + b_i = 0 \quad (1)$$

where $(\cdot)_{,j} = \partial(\cdot)/\partial x_j$, σ_{ij} is the stress field corresponding to the displacement field u_i ($i = 1$ to 2) and b_i is the body force. The boundary conditions are

$$\begin{aligned} T_i &= \sigma_{ij} n_j = T_{0i} \quad \text{on } \Gamma_T \\ u_i &= U_{0i} \quad \text{on } \Gamma_U \end{aligned} \quad (2)$$

where Γ_T is the natural boundary, Γ_U is the essential boundary, T_i are the tractions, U_{0i} and T_{0i} are known functions, n_j are the components of a unit vector \mathbf{n} out-

ward normal to Γ , and $\Gamma = \Gamma_U \cup \Gamma_T$.

If N_T nodes locate within Ω and Ω_S represents a local quadrature domain for a node \mathbf{x}_I ($I = 1$ to N_T), a local weak form of Equation (1) is

$$\int_{\Omega_S} (\sigma_{ij,j} + b_i) w_I d\Omega = 0 \quad (3)$$

where w_I is the test function associated with \mathbf{x}_I . Subsequently, this study similarly manipulates a published radial basis function-based interpolation formula [5] to construct the meshfree shape function N . Since the resulting N satisfies the Kronecker delta function property ($\delta_{IJ} = 0$ for $I \neq J$, $\delta_{IJ} = 1$ for $I = J$, and I, J denote the I -th and J -th nodes), Equation (3) contains neither Lagrangian multipliers nor penalty parameters for imposing the essential boundary condition. Further simplifying Equation (3) by the divergence theorem results in

$$\begin{aligned} & \int_{\Omega_S} \sigma_{ij} w_{I,j} d\Omega - \oint_{L_S} w_I T_i d\Gamma - \oint_{\Gamma_{SU}} w_I T_i d\Gamma \\ &= \oint_{\Gamma_{ST}} w_I T_{0i} d\Gamma + \int_{\Omega_S} b_i w_I d\Omega \end{aligned} \quad (4)$$

where $\Gamma_{ST} = \Omega_S \cap \Gamma_T$, $\Gamma_{SU} = \Omega_S \cap \Gamma_U$, $L_S = \Gamma_S - \Gamma_{ST} - \Gamma_{SU}$, and Γ_S is the boundary of Ω_S . Theoretically speaking, the shape of Ω_S can be arbitrary in computing Equation (4). However, choosing each Ω_S as a rectangular centered at \mathbf{x}_I ($I = 1$ to N_T) can simplify the numerical integration of Equation (4). In addition, Ω_S for \mathbf{x}_I ($I = 1$ to N_T) may be different from an interpolation domain Ω_Q for approximating an unknown or a random field in the neighborhood of the same node. The difference between Ω_S and Ω_Q is further illustrated in **Figure 1**. Also different in terpolation domains or points may be chosen for approximating an unknown or representing a random field.

Now substituting $w_I(\mathbf{x}) = H(\mathbf{x}) = c$ ($\mathbf{x} \in \Omega_S$) and $w_I(\mathbf{x}) = 0$ ($\mathbf{x} \notin \Omega_S$) ($I = 1$ to N_T) [7] into Equation (4) results in

$$-\oint_{L_S} T_i d\Gamma - \oint_{\Gamma_{SU}} T_i d\Gamma = \oint_{\Gamma_{ST}} T_{0i} d\Gamma + \int_{\Omega_S} b_i d\Omega \quad (5)$$

where H denotes the Heaviside step function, and c is an arbitrary constant ($c = 1$ is used in the succeeding study). Equation (5) outlines a distinguishing characteristic of the MLPG5 scheme. If the last term of this equation van-

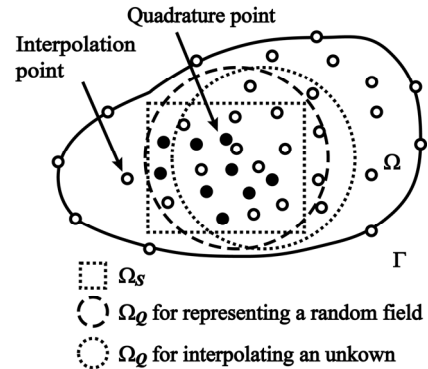


Figure 1. Difference between Ω_S and Ω_Q .

ishes, this equation contains no domain integrals. Therefore, if Equation (5) is adopted to derive a spectral stochastic meshless local Petrov-Galerkin formulation, computing the resulting spectral stochastic meshless local Petrov-Galerkin formulation is more time-saving than computing the published spectral stochastic meshless local Petrov-Galerkin formulation [5].

Moreover, substituting

$T_i = \sigma_{ij} n_j = (\lambda \delta_{ij} \varepsilon_{kk} + 2G \varepsilon_{ij}) n_j$ into Equation (5) yields

$$\begin{aligned} & -\oint_{L_S} nDBud\Gamma - \oint_{\Gamma_{SU}} nDBud\Gamma \\ & = \oint_{\Gamma_{ST}} \mathbf{T}_0 d\Gamma + \int_{\Omega_S} \mathbf{b} d\Omega \end{aligned} \quad (6)$$

where λ is the Lamè constant, G is the shear modulus, $\mathbf{u} = [u_1, u_2]^T$, $\mathbf{T}_0 = [T_{01}, T_{02}]^T$, $\mathbf{b} = [b_1, b_2]^T$, and

$$\mathbf{n} = \begin{bmatrix} n_1 & 0 & n_2 \\ 0 & n_2 & n_1 \end{bmatrix}, \quad \mathbf{D} = \begin{bmatrix} \lambda + 2G & \lambda & 0 \\ \lambda & \lambda + 2G & 0 \\ 0 & 0 & G \end{bmatrix} \quad (7)$$

$$\mathbf{B} = \begin{bmatrix} \frac{\partial}{\partial x_1} & 0 \\ 0 & \frac{\partial}{\partial x_2} \\ \frac{\partial}{\partial x_2} & \frac{\partial}{\partial x_1} \end{bmatrix}$$

Next, similarly manipulating a published radial basis function-based interpolation formula [5], \mathbf{u} over Ω_Q for a node is approximated by

$$\begin{aligned} \mathbf{u} &= \mathbf{N}^T \mathbf{U} = \begin{bmatrix} \mathbf{R}^T & \mathbf{p}^T \end{bmatrix} \begin{Bmatrix} \mathbf{U} \\ \mathbf{0} \end{Bmatrix} \\ &= \begin{bmatrix} \mathbf{R}^T & \mathbf{p}^T \end{bmatrix} \begin{bmatrix} \mathbf{R}_0 & \mathbf{P}_0 \\ \mathbf{P}_0^T & \mathbf{0} \end{bmatrix}^{-1} \begin{Bmatrix} \mathbf{U} \\ \mathbf{0} \end{Bmatrix} \end{aligned} \quad (8)$$

where $\mathbf{N}^T = [N_1, N_2, \dots, N_M]$, $\mathbf{U} = [u_1, u_2, \dots, u_M]^T$, M is the total number of nodes within an Ω_Q , the subscript i is the i -th node, $\mathbf{R}^T = [R_1, R_2, \dots, R_M]$, $\mathbf{p}^T = [p_1, p_2, \dots, p_m]$ is a complete monomial basis of order m , R_i , $i = 1$ to M represent the radial basis function, and

$$\mathbf{R}_0 = \begin{bmatrix} R_1(r_1) & R_2(r_1) & \cdots & R_M(r_1) \\ R_1(r_2) & R_2(r_2) & \cdots & R_M(r_2) \\ \vdots & \vdots & \ddots & \vdots \\ R_1(r_M) & R_2(r_M) & \cdots & R_M(r_M) \end{bmatrix} \quad (9a)$$

$$\mathbf{P}_0 = \begin{bmatrix} p_1(\mathbf{x}_1) & p_2(\mathbf{x}_1) & \cdots & p_m(\mathbf{x}_1) \\ p_1(\mathbf{x}_2) & p_2(\mathbf{x}_2) & \cdots & p_m(\mathbf{x}_2) \\ \vdots & \vdots & \ddots & \vdots \\ p_1(\mathbf{x}_M) & p_2(\mathbf{x}_M) & \cdots & p_m(\mathbf{x}_M) \end{bmatrix} \quad (9b)$$

in which \mathbf{x}_1 to \mathbf{x}_M represent those M nodes within Ω_Q for \mathbf{x}_I , and r_i to r_M represents the Euclidean distance between \mathbf{x}_I and each node within Ω_Q for \mathbf{x}_I . Constructing \mathbf{N} for further details can be seen in the published study [5].

Substituting Equation (8) into Equation (6) and writing the resulting expressions more succinctly in matrix algebra yield

$$\mathbf{K}_I \mathbf{u}_I = \mathbf{F}_I \quad (10)$$

where \mathbf{K} and \mathbf{F} are; respectively, the stiffness and force matrices, the subscript I represents the contribution to \mathbf{K} or \mathbf{F} at \mathbf{x}_I ($I = 1$ to N_T), $\mathbf{u}_I = [u_1, u_2, \dots, u_M]^T$, \mathbf{K}_I and \mathbf{F}_I are derived by

$$\begin{cases} \mathbf{K}_I = -\oint_{L_S} nDB(N)d\Gamma - \oint_{\Gamma_{SU}} nDB(N)d\Gamma \\ \mathbf{F}_I = \oint_{\Gamma_{ST}} \mathbf{T}_0 d\Gamma + \int_{\Omega_S} \mathbf{b} d\Omega \end{cases} \quad (11)$$

where the subscripts i and j denote i -th and j -th node within Ω_Q for \mathbf{x}_I ($I = 1$ to N_T); respectively and

$$\mathbf{B}(\mathbf{N}) = \begin{bmatrix} \frac{\partial \mathbf{N}}{\partial x_1} & 0 \\ 0 & \frac{\partial \mathbf{N}}{\partial x_2} \\ \frac{\partial \mathbf{N}}{\partial x_2} & \frac{\partial \mathbf{N}}{\partial x_1} \end{bmatrix} \quad (12)$$

Repeatedly deriving Equation (10) for all N_T nodes and assembling all the resulting expressions based on a global numbering system yield

$$\mathbf{K}_{(2N_T \times 2N_T)} \mathbf{u}_{(2N_T \times 1)} = \mathbf{F}_{(2N_T \times 1)} \quad (13)$$

Since this study accounts for the uncertainty in the spatial variability of mechanical properties in predicting the structural failure probability p_f , the generalized polynomial chaos expansion is introduced to represent random mechanical properties. The next section presents the relevant derivation.

3. Spectral Stochastic Meshless Local Petrov-Galerkin Formulation

Observing the derivation of Equation (13) needs mechanical properties G and λ . Thus, the generalized polynomial chaos expansions of G and λ are [5]

$$G = \sum_{i=0}^{N_{PC}} \hat{G}_i \Psi_i(\boldsymbol{\xi}) \quad \text{and} \quad \lambda = \sum_{i=0}^{N_{PC}} \hat{\lambda}_i \Psi_i(\boldsymbol{\xi}) \quad (14)$$

where $\boldsymbol{\xi} = (\xi_{i_1}, \xi_{i_2}, \dots, \xi_{i_n})$, Ψ_i represent the multivariate orthogonal polynomial of $\boldsymbol{\xi}$, $\xi_{i_1}, \xi_{i_2}, \dots, \xi_{i_n}$ denote multi-dimensional uncorrelated random variables having zero mean and unit variance (for facilitating the computation of mean values and standard deviations of G and λ), N_{PC} is equal to $(n + P)!/n!P! - 1$, P is the highest order of Ψ , and n is the total number of uncorrelated random

variables.

For facilitating the construction of Equation (14), Ψ_0 , \hat{G}_0 , and $\hat{\lambda}_0$ are, respectively, set to 1, μ_G , and μ_λ in which μ_G , and μ_λ are mean values of G and λ , respectively. Furthermore, computing \hat{G}_i , and $\hat{\lambda}_i$ ($i = 1$ to N_{PC}) needs the orthogonal relationship, $\langle \Psi_i, \Psi_j \rangle = \langle \Psi_i^2 \rangle \delta_{ij}$ ($i, j = 0$ to N_{PC}) in which $\langle \cdot \rangle$ is the ensemble average. For example, \hat{G}_i ($i = 0$ to N_{PC}) are computed by

$$\hat{G}_i = \frac{\langle G \Psi_i \rangle}{\langle \Psi_i^2 \rangle} \quad (15)$$

where $\langle \cdot \rangle$ is computed as follows: If f and g are two functions, $\langle \cdot \rangle$ is computed by

1) Continuous case:

$$\begin{aligned} & \langle f(\xi), g(\xi) \rangle \\ &= \int \int \dots \int f(\xi) g(\xi) W(\xi_{i_1}) \dots W(\xi_{i_n}) d\xi_{i_1} \dots d\xi_{i_n} \end{aligned} \quad (16a)$$

2) Discrete case:

$$\begin{aligned} & \langle f(\xi), g(\xi) \rangle \\ &= \sum_{\xi_{i_1}} \sum_{\xi_{i_2}} \dots \sum_{\xi_{i_n}} f(\xi) g(\xi) W(\xi_{i_2}) \dots W(\xi_{i_n}) \end{aligned} \quad (16b)$$

where $W(\xi_{i_1}) \dots W(\xi_{i_n})$ are the weighting functions. Since the succeeding study focuses on the continuous random fields, **Table 1** [6] lists examples of orthogonal polynomials, statistical distributions and weighting functions to generate Ψ_i ($i = 0$ to ∞), $\xi_{i_1} \dots \xi_{i_n}$, and $W(\xi_{i_1}) \dots W(\xi_{i_n})$; respectively.

Substituting Equation (14) into Equation (11) yields

$$\begin{aligned} \mathbf{K}_I &= \sum_{L=0}^{N_{PC}} \left[-\oint_{L_S} \mathbf{n} \mathbf{D}_L \mathbf{B}(N) d\Gamma - \oint_{\Gamma_{SU}} \mathbf{n} \mathbf{D}_L \mathbf{B}(N) d\Gamma \right] \\ &= \sum_{L=0}^{N_{PC}} (\hat{\mathbf{K}}_I)_L \Psi_L \end{aligned} \quad (17)$$

in which \mathbf{D}_L represents the computation of \mathbf{D} using \hat{G}_L and $\hat{\lambda}_L$ ($L = 0$ to M) and

$$(\hat{\mathbf{K}}_I)_L = -\oint_{L_S} \mathbf{n} \mathbf{D}_L \mathbf{B}(N) d\Gamma - \oint_{\Gamma_{SU}} \mathbf{n} \mathbf{D}_L \mathbf{B}(N) d\Gamma \quad (18)$$

Since the expressions of \mathbf{F}_I doesn't contain G and λ , substituting the generalized polynomial chaos expansions

Table 1. Examples of polynomials and corresponding weighting functions and statistical distributions for generating the generalized polynomial chaos [6].

Distribution	Polynomial	$W(\xi)$	Interval
Gaussian	Hermite $H_n(x)$	$\exp(-\xi^2)$	$(-\infty, \infty)$
gamma	Laguerre $L_n(x)$	$\exp(-\xi)$	$[0, \infty]$
beta	Jacobi $G_n(p, q, x)$	$(1-\xi)^{p-q} \xi^{q-1}$	$[a, b]$
uniform	Legendre $P_n(x)$	1	$[a, b]$

Note that [a, b] denotes a specific interval.

of G and λ into \mathbf{F}_I is unnecessary. Meanwhile, the generalized polynomial chaos expansion of \mathbf{u} is

$$\mathbf{u} = \sum_{J=0}^{N_{PC}} \hat{\mathbf{u}}_J \Psi_J \quad (19)$$

Substituting Equations (17) and (19) into Equation (11) results in

$$\sum_{L=0}^{N_{PC}} \sum_{J=0}^{N_{PC}} \hat{\mathbf{K}}_L \hat{\mathbf{u}}_J \Psi_L \Psi_J = \sum_{L=0}^{N_{PC}} \hat{\mathbf{F}}_L \Psi_L \quad (20)$$

Requiring the residual resulting from a finite representation of \mathbf{u} (*i.e.* truncating $\hat{\mathbf{u}}_J \Psi_J$,

$J = N_{PC} + 1, N_{PC} + 2, \dots$) to be orthogonal to the approximation space spanned by Ψ_J yields

$$\sum_{L=0}^{N_{PC}} \sum_{J=0}^{N_{PC}} \hat{\mathbf{K}}_L \hat{\mathbf{u}}_J \langle \Psi_L \Psi_J \Psi_k \rangle = \sum_{L=0}^{N_{PC}} \hat{\mathbf{F}}_L \langle \Psi_L \Psi_k \rangle \quad (21)$$

in which $k = 0$ to N_{PC} . Solving Equation (21) can obtain $\hat{\mathbf{u}}_J$ ($J = 0$ to N_{PC}). Collecting the resulting $\hat{\mathbf{u}}_J$ can construct the generalized polynomial chaos expansion of \mathbf{u} .

4. First Order Reliability Method

This study introduces structural reliability assessment problems to evaluate the performance of Equation (21). Estimating this structural reliability follows the first-order reliability method [9]; therefore, this section summarizes the first-order reliability method.

Given a traction \mathbf{T}_0 bearing on a structure subjected to the uncertainty in the spatial variability of G and λ , a vector \mathbf{X} having components G and λ at all N_T nodes is created. In addition, a performance state function $g(\mathbf{X})$ is defined to identify the failure ($g(\mathbf{X}) < 0$) and safe states ($g(\mathbf{X}) > 0$) of the structure. For example, a book [11] emphasizes \mathbf{T}_0 and its resistance \mathbf{R} ; thus, $g(\mathbf{X})$ is

$$g(\mathbf{X}) = \mathbf{T}_0 - \mathbf{R} \quad (22)$$

Moreover, a space of different \mathbf{X} values is plotted and the location of $g(\mathbf{X})$ is marked. **Figure 2** [12] illustrates the special case of $\mathbf{X} = (X_1, X_2)$. In this figure, suppose the point A denotes the point (μ_{X_1}, μ_{X_2}) and the structure is safe at this point. Observing **Figure 2** can know that the shortest distance between point A and $g(\mathbf{X})$ sizes the range of \mathbf{X} values within which a safe structural design is expected. Extending this observation, the shortest distance between $(\mu_{X_1}, \mu_{X_2}, \dots, \mu_{X_{2N_T}})$ and $g(\mathbf{X})$ sizes the range of \mathbf{X} values within which a safe structural design is expected. Hasofer and Lind (1974) [9] defined the shortest distance between $(\mu_{X_1}, \mu_{X_2}, \dots, \mu_{X_{2N_T}})$ and $g(\mathbf{X})$, in units of directional standard deviations as the reliability index β . They concluded that searching β is a constrained optimization problem in the form as [12]

$$\begin{aligned} \beta &= \min_{\mathbf{X} \in F} \sqrt{(\mathbf{X} - \boldsymbol{\mu})^T \mathbf{C}^{-1} (\mathbf{X} - \boldsymbol{\mu})} \\ &\text{subjected to } g(\mathbf{X}) = 0 \end{aligned} \quad (23)$$

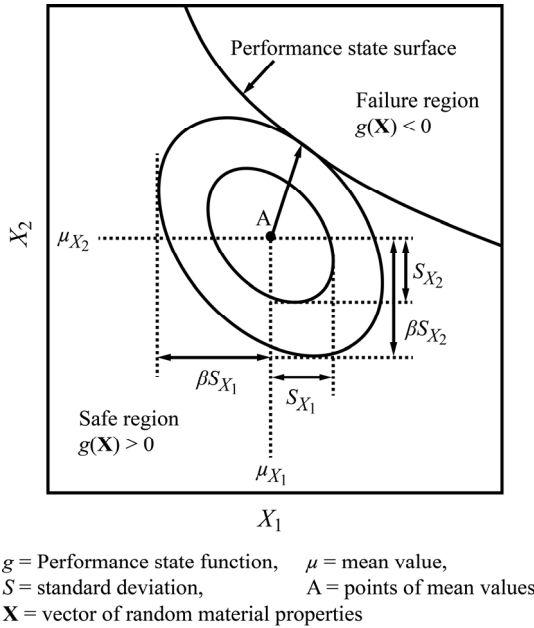


Figure 2. Search of the reliability index β [12].

where F denotes the failure region on the space of \mathbf{X} , $\boldsymbol{\mu} = (\mu_{X_1}, \mu_{X_2}, \dots, \mu_{X_{2N_T}})$, and \mathbf{C} is the covariance matrix.

A number of algorithms have been developed to solve Equation (23) or similar equations. This study chooses a popular algorithm suggested by Lowe and Tang [12]. Briefly, this algorithm is based on the Rackwitz-Fiessler equivalent normal transformation [13] but the concepts of coordinate transformation and frame-of-reference rotation are not applied. Correlation is accounted for by setting up the quadratic form directly. Similarly manipulating the previous study [12], three steps are performed to solve Equation (23):

1) Modify Equation (23) with standard normal random variables. Transform the vector \mathbf{X} into a new vector of \mathbf{Y} having standard normal random variables Y_i ($i = 1$ to $2N_T$) in the form as

$$Y_i = \frac{X_i - \mu_{X_i}}{S_{X_i}} = \Phi^{-1}[CDF(X_i)] \quad (24)$$

in which $\Phi(X) = \frac{1}{\sqrt{2\pi}} \int_{-\infty}^X \exp(-\zeta^2/2) d\zeta$ is the cumulative probability function of a standard normal distribution, CDF is the cumulative probability function computed at X_i . Using the new vector \mathbf{Y} , Equation (23) is modified to

$$\beta = \min_{\mathbf{X} \in F} \sqrt{\mathbf{Y}^T \boldsymbol{\rho}^{-1} \mathbf{Y}} \quad \text{subjected to } g(\mathbf{X}) = 0 \quad (25)$$

in which $\boldsymbol{\rho}$ is the correlation matrix evaluated at \mathbf{Y} .

2) Start from $Y_i = 0$ ($i = 1$ to $2N_T$) (or $X_i = \mu_{X_i}$) to search the \mathbf{X} value causing $g(\mathbf{X}) = 0$. In searching such an \mathbf{X} value, increase \mathbf{Y} values and calculate the corresponding \mathbf{X} value by **Table 2** [12]. Note that this table is edited

Table 2. Obtaining X_i from Y_i based on $CDF(X_i) = \Phi(Y_i)$ [12].

Distribution	$X_i = CDF^{-1}(F(Y_i))$
Normal	$X_i = \mu_{X_i} + Y_i S_{X_i}$
Lognormal	$X_i = \exp(\lambda + \zeta Y_i)$, $\zeta = \sqrt{\ln \left[1 + \left(\frac{S_{X_i}}{\mu_{X_i}} \right)^2 \right]}$ $\lambda = \ln \mu_{X_i} - 0.5 \zeta^2$
Extreme value	$X_i = \eta - \frac{\ln[-\ln(\Phi(Y_i))]}{\alpha}$, $\zeta = \frac{\pi}{\sqrt{6} S_{X_i}}$ $\eta = \mu_{X_i} - 0.5772/\alpha$
Exponential	$X_i = -\mu_{X_i} \ln[1 - \Phi(Y_i)]$
Uniform	$X_i = a + (b - a)\Phi(Y_i)$, $f_x(X) = \begin{cases} 1/(b-a) & X \in [a, b] \\ 0 & \text{otherwise} \end{cases}$

f_x = probability density function.

by choosing those probability distributions, which may be applied in the current study.

3) To incorporate with a spectral stochastic meshless local Petrov-Galerkin FORTRAN code, a VA10AD subroutine [14] is introduced to automate the above two steps.

After finding the \mathbf{X} value causing $g(\mathbf{X}) = 0$ and computing the corresponding β value from Equation (25), the structural failure probability p_f is estimated by

$$p_f = CDF(\mathbf{X}) = \int_{g(\mathbf{X}) \leq 0} PDF(\mathbf{X}) d\mathbf{X} \quad (26)$$

$$\approx \Phi(-\beta) = 1 - \Phi(\beta)$$

where PDF is the probability density function.

5. Results and Discussions

Two benchmark problems are introduced to evaluate the performance of Equation (21). As a comparison, the spectral stochastic finite element method is applied to the same problems. The FERUM package [15] is adopted to generate spectral stochastic finite element results. The first benchmark problem involves bending of a cantilever beam by a parabolically distributed traction at its free end. The second benchmark problem involves bending of a dam caused by the fluid pressure. Except for inspecting the accuracy of spectral stochastic meshless local Petrov-Galerkin-based predicted p_f , two different radial basis functions are; respectively, adopted to construct N in solving those two problems; thus, the effects of different radial basis functions on the accuracy of spectral stochastic meshless local Petrov-Galerkin results can be observed.

5.1. Bending of a Cantilever Beam by a Parabolically Distributed Traction

Suppose the cantilever beam has the length L , width h , and unit thickness. **Figure 3** illustrates the layout of this cantilever beam and boundary conditions in which Q denotes the integration of parabolically distributed traction along the x_2 direction and the point B is subsequently used to define the performance state function $g(\mathbf{X})$. If any uncertainty is neglected, the analytical solution of u_2 is [10]

$$u_2 = -\frac{Q(\lambda + G)}{6G(3\lambda + 2G)I} \left\{ \frac{3\lambda x_2^2(L - x_1)}{2(\lambda + G)} + \left[4 + \frac{5\lambda}{2(\lambda + 2G)} \right] \frac{h^2 x_1}{4} (3L - x_1) x_1^2 \right\} \quad (27)$$

where $I = h^3/12$ is the moment of inertia and Q is integration of the parabolically distributed traction along the x_2 direction. Since only the analytical solution of u_2 is adopted subsequently to implement the Monte Carlo simulation, analytical solutions of u_1 and σ_{ij} ($i, j = 1$ to 2) are not listed here. Interested readers can find these analytical solutions in the book [10].

Nevertheless, this study accounts for the uncertainty in random G and λ in predicting p_f . Assume G and λ vary according to

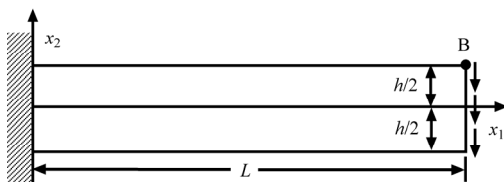
$$G = \mu_G [1 + \alpha_G(\mathbf{x})] \quad \text{and} \quad \lambda = \mu_\lambda [1 + \alpha_\lambda(\mathbf{x})] \quad (28)$$

where α_G and α_λ are two homogeneous Gaussian random fields with zero mean and having the following covariance functions C_G and C_λ :

$$C_G = \text{cov}[G(x_1, x_2), G(x_1 + \zeta_1, x_2 + \zeta_2)] = S_G^2 \exp\left(-\frac{|\zeta_1|}{d_1 L} - \frac{|\zeta_2|}{d_2 h}\right) \quad (29a)$$

$$C_\lambda = \text{cov}[\lambda(x_1, x_2), \lambda(x_1 + \zeta_1, x_2 + \zeta_2)] = S_\lambda^2 \exp\left(-\frac{|\zeta_1|}{d_3 L} - \frac{|\zeta_2|}{d_4 h}\right) \quad (29b)$$

in which cov represents the covariance, (x_1, x_2) and $(x_1 +$



$$\begin{aligned} T_i(x_2 = -h/2) &= 0 & T_2(x_1 = L) &= -Q & u_i(x_i = 0) &= 0 \\ T_i(x_2 = h/2) &= 0 & & & & \\ T_1(x_1 = L) &= 0 & & & & \end{aligned} \quad \begin{array}{l} \text{(parabolically} \\ \text{distributed)} \end{array}$$

Figure 3. Bending of a cantilever beam by a parabolically distributed at its ends (not to scale, $i = 1$ to 2).

$\zeta_1, x_2 + \zeta_2)$ are two points on the cantilever beam, S_G and S_λ are; respectively, standard deviations of G and λ , and d_i ($i = 1$ to 4) are four correlation parameters.

To predict p_f of the cantilever beam with the uncertainty in random G and λ , essential data are listed below

1) Define the problem domain Ω as $0 \leq x_1 \leq L$ and $-h/2 \leq x_2 \leq h/2$.

2) Generate two cases of meshless discretizations and one case of finite element discretization. **Figure 4** illustrates these meshless (top and middle sub-figures) and finite element discretizations (bottom sub-figure) in which the meshless discretization of randomly located nodes (middle sub-figure) is obtained by randomly distributing the meshless discretization of equally spaced nodes (bottom sub-figure).

3) Experiment to represent G , λ , and \mathbf{u} by the Laguerre polynomial chaos.

4) Set a complete monomial basis $\mathbf{p}^T = [1, x_1, x_2]$ ($m = 3$). Setting such a low-order of p is intentional. Observing the accuracy of corresponding numerical results is desired.

5) Construct N by the Gaussian radial basis function; that is, $R_i = \exp(-\alpha_c r_i^2)$ ($i = 1$ to M) where $\alpha_c (\geq 0)$ is a shape parameter.

6) Choose each Ω_Q as a circle centered at a point and each Ω_S as a rectangular centered at a node. The length and width of each Ω_S and radius of each Ω_Q are set subsequently.

7) Define the performance state function $g(\mathbf{X})$ by

$$g(\mathbf{X}) = u_\delta - u_{2,B} \quad (30)$$

where u_δ is a threshold of displacement and the subscript B denotes the point B in **Figure 3**.

8) Generate Monte Carlo simulation results to serve as the accuracy standard in comparing spectral stochastic finite element-based and spectral stochastic meshless local Petrov-Galerkin-based predicted p_f . Following a book [11] the first step of implementing a Monte Carlo simulation is sampling of G and λ according to Equation (28). Each sample of G and λ are then substituted into

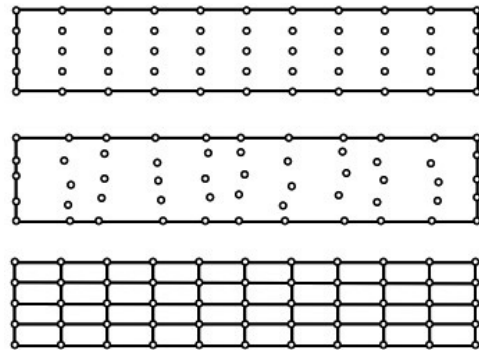


Figure 4. Meshless and finite element discretizations for analyzing the first benchmark problem.

Equation (27) to compute a sample of $u_{2,B}$. If N_{sample} is the total number of samples of $u_{2,B}$ and $N(g(\mathbf{X}) \leq 0)$ is the total number of samples of $u_{2,B}$ causing the structural failure, p_f is computed by

$$p_f = \frac{N(g(\mathbf{X}) \leq 0)}{N_{\text{sample}}} \quad (31)$$

Moreover, the resulting p_f can be inverted to compute the reliability index β . If G and λ are sufficiently sampled, the Monte Carlo simulation-based p_f and β approach their exact values.

9) Unless otherwise stated, the following parameters are adopted: $L = 48$ m, $h = 12$ m, $N_{PC} = 10$, $\mu_G = 11.5$ MPa, $\mu_\lambda = 17.3$ MPa, $\alpha_c = 0.03$, $H_s = 9.6$ m, $B_s = 6$ m, $r_Q = 6$ m, $N_{\text{sample}} = 10^6$, $N_q = 16$, $d_i = 1$ ($i = 1$ to 4), $Q = 10^3$ kN where H_s and B_s are; respectively, the height and width of each Ω_S , r_Q is the radius of each Ω_Q , and N_q is the total number of quadrature points in each Ω_S or finite element.

Moreover, in order to state quantitatively the accuracy of spectral stochastic meshless local Petrov-Galerkin or spectral stochastic finite element results, two error estimators Δ and δ are defined below

$$\Delta(\%) = \frac{(p_f)_{MCS} - (p_f)_{SSMLPG}}{(p_f)_{MCS}} \quad (32)$$

$$\delta(\%) = \frac{(p_f)_{MCS} - (p_f)_{SSFEM}}{(p_f)_{MCS}}$$

in which the subscripts *MCS*, *SSMLPG*, and *SSFEM* denote the Monte Carlo simulation, spectral stochastic meshless local Petrov-Galerkin and spectral stochastic finite element methods; respectively.

Figure 5 compares variation of the predicted PDF of u_2 at the point B versus different prediction methods

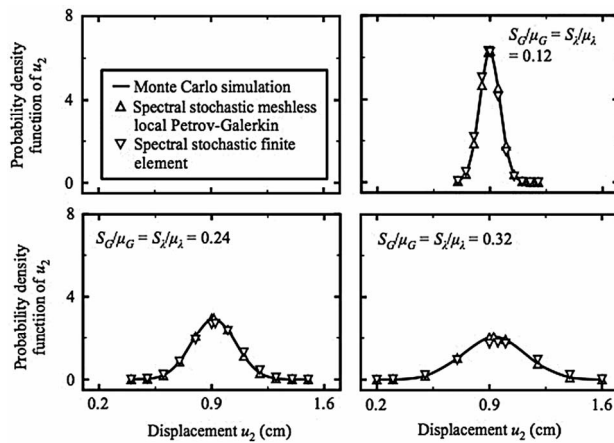


Figure 5. Variation of the predicted probability density function of u_2 at the point B versus different S_G/μ_G and S_λ/μ_λ values (First benchmark problem, meshless discretization: the top sub-figure of Figure 4, $d_1 = d_2 = d_3 = d_4 = 1$).

and $S_G/\mu_G = S_\lambda/\mu_\lambda = 0.12, 0.24, 0.32$. **Figure 6** (in the next page) presents variation of the predicted p_f at the point B versus different u_δ values, prediction methods, and $S_G/\mu_G = S_\lambda/\mu_\lambda = 0.12, 0.24, 0.32$. Furthermore, **Table 3** compares the time spent to produce the spectral stochastic meshless local Petrov-Galerkin-based and Monte Carlo simulation-based predicted p_f with $S_G/\mu_G = S_\lambda/\mu_\lambda = 0.12$.

Benefiting from adopting the MLPG5 scheme to derive a spectral stochastic meshless local Petrov-Galerkin formulation, **Table 3** indicates that generating spectral stochastic meshless local Petrov-Galerkin results is considerably time-saving, even if the Monte Carlo simulation is implemented using analytical solutions. Meanwhile, **Figure 5** illustrates the necessity of predicting \mathbf{u} with the uncertainty in the spatial variability of G and λ . When the S_G/μ_G and S_λ/μ_λ values increase, the standard deviation of u_2 increase; thus, obtaining the predicted u_2 , which is different from its mean value, becomes more and more possible. In addition, **Figure 6** presents that the spectral stochastic meshless local Petrov-Galerkin method predicts more accurate p_f than the spectral stochastic finite element method does. For example, if computing Δ and δ values with $S_G/\mu_G = S_\lambda/\mu_\lambda = 0.12$, the resulting Δ value approximately peaks at 0.36 %; whereas, the resulting δ value peaks about at 13.97 %.

Nevertheless, the performance of both Equation (21)

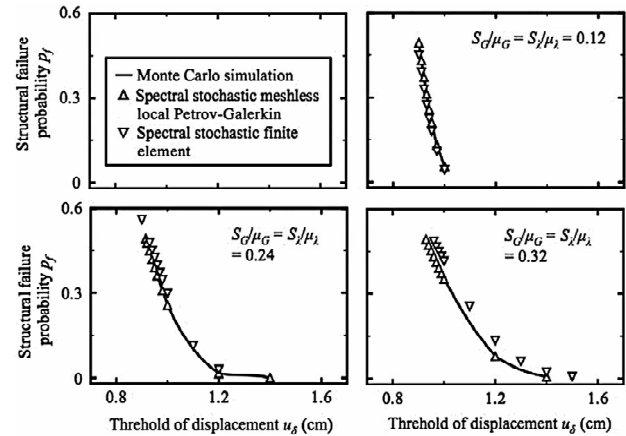


Figure 6. Variation of the predicted structural failure probability p_f at the point B versus different S_G/μ_G and S_λ/μ_λ values (first benchmark problem, meshless discretization: the top sub-figure of Figure 4, $d_1 = d_2 = d_3 = d_4 = 1$).

Table 3. Comparison of the time spent to generate Monte Carlo simulation and spectral stochastic meshless local Petrov-Galerkin results*.

Monte Carlo Simulation	Spectral stochastic meshless local Petrov-Galerkin method
281 seconds	1.5 seconds

*On a MacBook Pro with an Intel Core i5 Processor, GFortran compiler.

and spectral stochastic finite element method becomes gradually unsatisfactory when S_G/μ_G and S_λ/μ_λ increases. If S_G/μ_G and S_λ/μ_λ values measure the degree of uncertainty, **Figure 6** outlines that the degree of uncertainty can apparently reduce the accuracy of predicted \mathbf{u} or p_f . Furthermore, observing Equations (29a) to (29b) can find that decreasing d_i ($i = 1$ to 4) values and increasing S_G/μ_G and S_λ/μ_λ values have similar effects on the accuracy of predicted \mathbf{u} or p_f .

Next, replacing Lauguerre polynomial chaos with Hermite polynomial chaos to represent G , λ , and \mathbf{u} , **Figure 7** compares spectral stochastic meshless local Petrov-Galerkin-based predicted p_f values versus different types of the polynomial chaos, $S_G/\mu_G = S_\lambda/\mu_\lambda = 0.12$, and different u_δ values.

Figure 7 implies the importance of preparing some pilot tests before choosing a specific type of polynomial chaos to represent a random field. Calculating Δ values using this figure finds that the performance of Lauguerre polynomial chaos is more satisfactory. If G and λ are represented using the Hermite polynomial chaos, the corresponding Δ value peaks at about 2.758%.

Next, replacing meshless discretization of equally spaced nodes (the top sub-figure of **Figure 4**) with meshless discretization of randomly located nodes (the middle sub-figure of **Figure 4**), **Figure 7** re-compares variation of Monte Carlo simulation-based and spectral stochastic meshless local Petrov-Galerkin-based predicted p_f values versus different u_δ values, and $S_G/\mu_G = S_\lambda/\mu_\lambda = 0.12$.

Computing the Δ value using data in **Figure 8** finds that the resulting Δ value peaks at about 2.367%. Consequently, Equation (21) still predicts p_f sufficiently accurately, even if a meshless distribution of discrete nodes is adopted. Moreover, in an attempt of more understanding the effects of different nodal spacings on the accu-

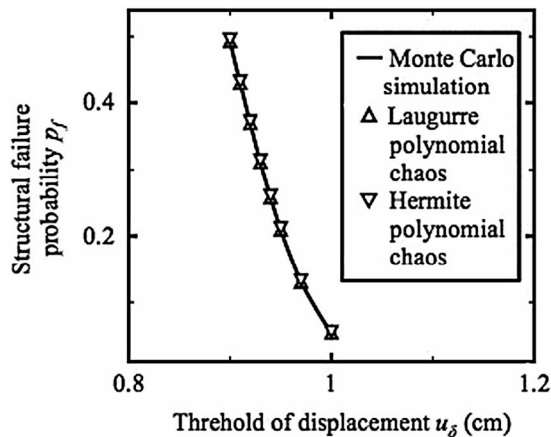


Figure 7. Variation of the predicted structural failure probability p_f at the point B versus different types of the polynomial chaos (first benchmark problem, meshless discretization: the upper sub-figure of **Figure 4**, $d_1 = d_2 = d_3 = d_4 = 1$).

racy of predicted p_f , the problem domain Ω is re-discretized using equally spaced nodes and $N_T = 27$ (3×9), 52 (4×13), 85 (5×17). **Figure 9** depicts the corresponding variation of Monte Carlo simulation-based and spectral stochastic meshless local Petrov-Galerkin-based predicted p_f versus different h values, $u_\delta = 0.95$ cm, and $S_G/\mu_G = S_\lambda/\mu_\lambda = 0.12$ where h denotes the spacing of any two connecting nodes.

Figure 9 reports that the effects of different h values on the accuracy of predicted p_f are not noticeable. For example, if the N_T value increases from 52 (3×9) to 85 (5×17), the corresponding Δ value only changes slightly; consequently, adopting more nodes for improving the accuracy of Monte Carlo simulation-based or spectral stochastic meshless local Petrov-Galerkin-based predicted p_f is laborious.

5.2. Bending of a Dam Caused by Fluid Pressure

Suppose the dam has the length L , width h , and unit thick-

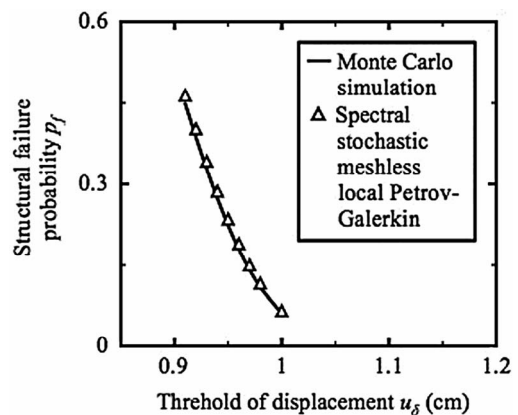


Figure 8. Variation of the predicted structural failure probability p_f at the point B versus randomly nodal distribution (first benchmark problem, meshless discretization: the middle sub-figure of **Figure 4**, $d_1 = d_2 = d_3 = d_4 = 1$).

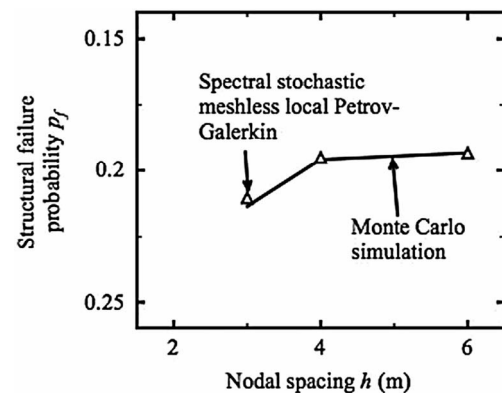


Figure 9. Variation of the predicted structural failure probability p_f at the point B versus different nodal spacing h (m) (First benchmark problem, meshless discretization: the upper sub-figure of **Figure 4**, $d_1 = d_2 = d_3 = d_4 = 1$).

ness. This dam is fixed at one end and subjected to fluid pressure. **Figure 10** illustrates the layout of problem domain Ω and boundary conditions in which C and D are subsequently used to define the performance state function and γ_f is the unit weight of fluid.

If any uncertainty is neglected, the analytical solutions of u_1 and u_2 are [10]

$$u_1 = \frac{(\lambda + G)x_2\gamma_f}{G(3\lambda + 2G)h^2} \left\{ (x_1^2 - L^2) \left(-x_2^2 + \frac{3h^2}{20} \right) + \frac{(x_1^3 - L^3)}{3} + \frac{\lambda(x_1^2 - L^2)\gamma_f}{4G(3\lambda + 2G)} \left[-\frac{1}{2} + \frac{x_2}{h} \left(\frac{2x_2^2}{h^2} - \frac{3}{2} \right) \right] \right\} \quad (33a)$$

$$u_2 = \frac{(\lambda + G)(x_1 - L)\gamma_f x_2}{2G(3\lambda + 2G)} \left\{ -1 + \frac{x_2}{h} \left(\frac{x_2^2}{h^2} - \frac{3}{2} \right) + \frac{\lambda\gamma_f x_2^2}{2G(3\lambda + 2G)h} \left[-\frac{(x_1^2 - L^2)}{2h} + \frac{(x_1 - L)}{2} \left(x_2^2 - \frac{3h^2}{10} \right) \right] \right\} \quad (33b)$$

However, suppose G and λ vary according to two uniform distributions:

$$\begin{aligned} G &= \mu_G [1 + S_G^2(\zeta_1 + \zeta_2)] \\ \lambda &= \mu_\lambda [1 + S_\lambda^2(\zeta_3 + \zeta_4)] \end{aligned} \quad (34)$$

where $-1 < \zeta_i$ ($i = 1$ to 4) < 1 represent four random variables.

To predict p_f of the dam with the uncertainty in random G and λ , the essential data are provided below:

1) Define the problem domain Ω as $-h/2 \leq x_2 \leq h/2$ and $0 \leq x_1 \leq L$.

2) Generate a meshless discretization and a finite element discretization. **Figure 11** presents these meshless

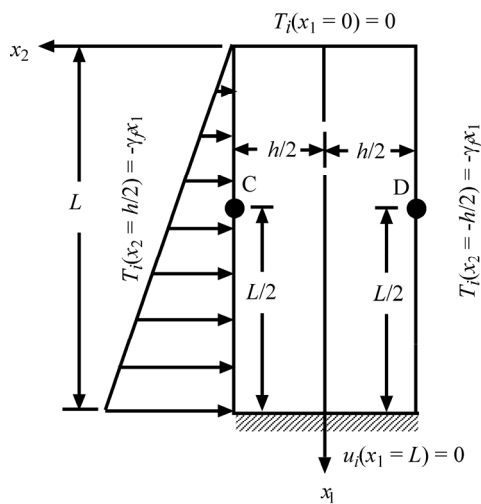


Figure 10. Bending of a dam caused by fluid pressure [10] (not to scale, $i = 1$ to 2).

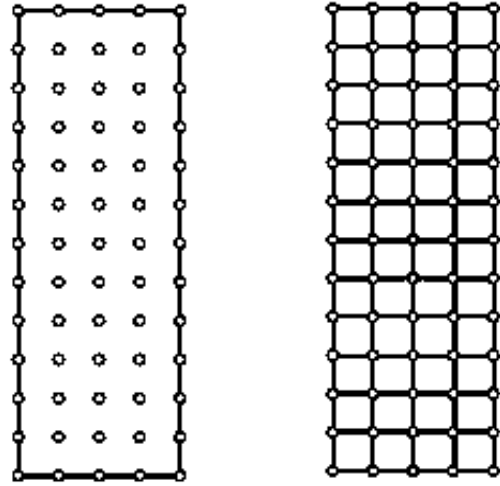


Figure 11. Meshless and finite element discretizations for analyzing the second benchmark problem.

and finite element discretizations.

3) Represent G , λ , and u_i ($i = 1$ to 2) by the Legendre polynomial chaos.

4) Still set a complete monomial basis $\mathbf{p}^T = [1, x_1, x_2]$ but adopt the multiquadric radial basis function to construct ϕ , that is, $R_i = [r_i^2 + (\alpha_c d_c)^2]^{-q}$ ($i = 1$ to M) where α_c (≥ 0) and q are two shape parameters and d_c is the characteristic length related to the nodal spacing in an Ω_Q .

5) Define two performance state functions $g_1(\mathbf{X})$ and $g_2(\mathbf{X})$ as follows:

$$g_1(\mathbf{X}) = u_{2,\delta} - u_{2,C} \quad (35a)$$

$$g_2(\mathbf{X}) = u_{1,\delta} - u_{1,D} \quad (35b)$$

where $u_{i,\delta}$ ($i = 1$ to 2) are two thresholds of displacements and the subscripts C and D denote the points C and D in **Figure 10**.

6) Similarly manipulate point (8) in Section 5.1 but replace Equation (27) with Equations (33a) to (33b) to generate the Monte Carlo simulation-based predicted p_f . The resulting Monte Carlo simulation-based predicted p_f serves as the accuracy standard in comparing the spectral stochastic meshless local Petrov-Galerkin and spectral stochastic finite element results.

7) Unless otherwise stated, the following data are used: $L = 30$ m, $h = 10$ m, $\gamma_f = 9.81$ kN/m³, $N_{PC} = 10$, $\mu_G = 11.5$ MPa, $\mu_\lambda = 17.3$ MPa, $\alpha_c = 1.0$, $d_c = 3.0$, $q = 1.03$, $H_S = 5$ m, $B_S = 5$ m, $r_Q = 5$ m, $N_{\text{sample}} = 10^6$, and $N_q = 16$.

Figure 12 (in the next page) compares variation of the p_f at the point C with respect to $S_G/\mu_G = S_\lambda/\mu_\lambda = 0.12, 0.24, 0.32$, different prediction methods and $u_{2,\delta}$ values.

Figure 13 (in the next page) compares variation of the p_f at the point D with respect to $S_G/\mu_G = S_\lambda/\mu_\lambda = 0.12, 0.24, 0.32$, different prediction methods and $u_{1,\delta}$ values.

Observing **Figure 12** confirms that the performance of

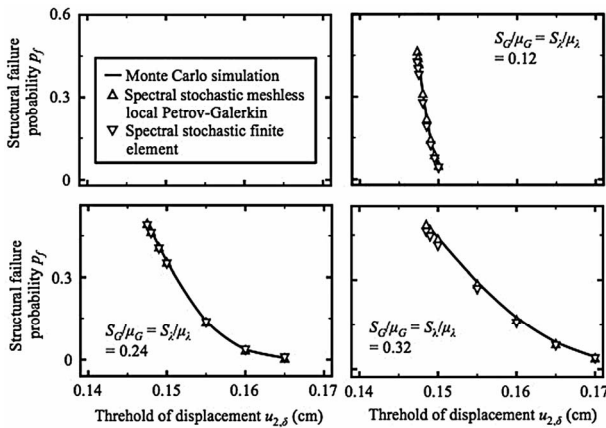


Figure 12. Variation of the predicted structural failure probability p_f at the point C versus different S_G/μ_G and S_λ/μ_λ values (Second benchmark problem).

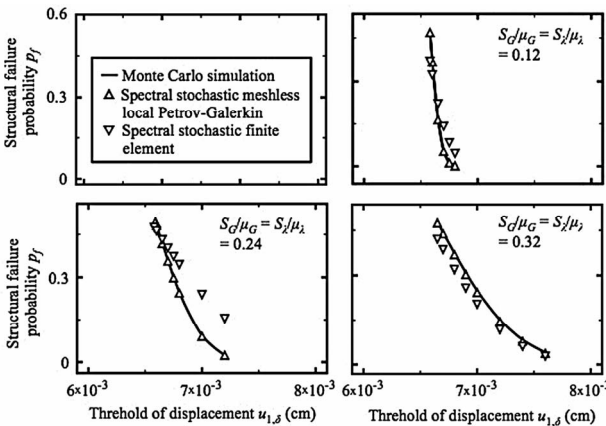


Figure 13. Variation of the predicted structural failure probability p_f at the point D versus different S_G/μ_G and S_λ/μ_λ values (Second benchmark problem).

spectral stochastic meshless local Petrov-Galerkin method is more satisfactory than the performance of spectral stochastic finite element method. Even if different statistical distributions are encountered, **Figures 6, 12, and 13** present the spectral stochastic meshless local Petrov-Galerkin results are more accurate than the spectral stochastic finite element results. In addition, careful inspection of spectral stochastic finite element results in **Figures 12 to 13** finds that the errors between Monte Carlo simulation and spectral stochastic finite element results majorly source from inaccurate spectral stochastic finite element-based predicted mean values of u at the points C and D. Resolving this problem may need high-order finite elements. But, to the author’s knowledge, similar experiences seem to be seldom seen.

6. Conclusions

Prior to the previous [5] and current studies, available stochastic numerical methods include the Monte Carlo

simulation, spectral stochastic finite element, and stochastic element-free Galerkin methods. The Monte Carlo simulation is simplest. As demonstrated in Sections 5.1 and 5.2, implementing the Monte Carlo simulation only needs deterministic solutions. Even so, as outlined by **Table 3**, completing the Monte Carlo simulation is still more time-consuming than generating the spectral stochastic meshless local Petrov-Galerkin results. Producing such results attributes to that the total number of samples for implementing a Monte Carlo simulation is usually very large.

Meanwhile, applying the spectral stochastic finite element method is easy, since numerous resources (computer software and experiences) are available. Nevertheless, based on these resources, this study finds that the spectral stochastic finite element results of some problems are less accurate than spectral stochastic meshless local Petrov-Galerkin results of the same problems. Sections 5.1 and 5.2 provide two examples.

Together with the previous study [5], the succeeding study provides a new alternative for solving stochastic boundary-value problems. This new stochastic numerical method is truly-meshless. As demonstrated in Sections 5.1 and 5.2, no finite elements or background cells for the numerical integration are created in applying the spectral stochastic meshless local Petrov-Galerkin method. However, the spectral stochastic meshless local Petrov-Galerkin method successfully spend less time but still predict the accurate structural failure probability p_f in Sections 5.1 and 5.2.

In conclusion, the spectral stochastic meshless local Petrov-Galerkin method is a time-saving tool for solving stochastic boundary-value problems.

REFERENCES

- [1] R. G. Ghanem and P. D. Spanos, “Stochastic Finite Elements: A Spectral Approach,” Revised Edition, Dover Publications, New York, 2012.
- [2] S. Rahman and B. N. Rao, “An Element-Free Galerkin Method for Probabilistic Mechanics and Reliability,” *International Journal of Solids and Structures*, Vol. 38, No. 50-51, 2001, pp. 9313-9330.
- [3] V. Papadoulous, G. Soimiris and M. Papadrakis, “Buckling Analysis of I-Section Portal with Stochastic Imperfections,” *Engineering Structures*, Vol. 47, 2013, pp. 54-66. [doi:10.1016/j.engstruct.2012.09.009](https://doi.org/10.1016/j.engstruct.2012.09.009)
- [4] K. Sepahvand, S. Marburg and H.-J. Hardtke, “Stochastic Free Vibration of Orthotropic Plates Using Generalized Polynomial Chaos Expansion,” *Journal of Sound and Vibration*, Vol. 331, No. 1, 2012, pp. 167-179. [doi:10.1016/j.jsv.2011.08.012](https://doi.org/10.1016/j.jsv.2011.08.012)
- [5] G. Y. Sheu, “Prediction of Probabilistic Settlements via Spectral Stochastic Meshless Local Petrov-Galerkin Method,” *Computers and Geotechnics*, Vol. 38, No. 4, 2011, pp. 407-415. [doi:10.1016/j.compgeo.2011.02.001](https://doi.org/10.1016/j.compgeo.2011.02.001)

- [6] D. Xiu and G. E. Karniadakis, "Modeling Uncertainty in Flow Simulations via Generalized Polynomial Chaos," *Journal of Computational Physics*, Vol. 187, No. 1, 2003, pp. 137-167. [doi:10.1016/S0021-9991\(03\)00092-5](https://doi.org/10.1016/S0021-9991(03)00092-5)
- [7] S. N. Atluri and T. Zhu, "A New Meshless Local Petrov-Galerkin (MLPG) Approach in Computational Mechanics," *Computational Mechanics*, Vol. 22, No. 2, 1998, pp. 117-127. [doi:10.1007/s004660050346](https://doi.org/10.1007/s004660050346)
- [8] S. N. Atluri and S. Shen, "The Meshless Local Petrov-Galerkin (MLPG) Method," Tech Science Press, Ecino, 2002.
- [9] A. M. Hasofer and N. C. Lind, "Exact and Invariant Second-Moment Code Format," *Journal of Engineering Mechanics ASCE*, Vol. 100, No. 1, 1974, pp. 1227-1238.
- [10] S. Timoshenko and J. N. H. Goodier, "Theory of Elasticity," 3rd Edition, McGraw-Hill Publishing Company, New York, 1970.
- [11] R. E. Melchers, "Structural Reliability Analysis and Prediction," 2nd Edition, John Wiley and Sons, England, 1999.
- [12] B. K. Low and W. H. Tang, "Efficient Spreadsheet Algorithm for First-Order Reliability Method," *Journal of Engineering Mechanics ASCE*, Vol. 133, No. 12, 2007, pp. 1378-1387. [doi:10.1061/\(ASCE\)0733-9399\(2007\)133:12\(1378\)](https://doi.org/10.1061/(ASCE)0733-9399(2007)133:12(1378))
- [13] R. Rackwitz and B. Fiessler, "Structural Reliability under Combined Random Load Sequences," *Computers and Structures*, Vol. 9, No. 5, 1978, pp. 484-494. [doi:10.1016/0045-7949\(78\)90046-9](https://doi.org/10.1016/0045-7949(78)90046-9)
- [14] R. Fletcher, "VA10AD Harwell Subroutine Library," A. E. R. E. Harwell, Oxfordshire, 1972.
- [15] B. Sudret and A. D. Kiureghian, "Stochastic Finite Elements and Reliability: A State-of-Art Report," Report No. UCB/SEMM-2000/08, University of California, Berkeley, 2000.